J. Plasma Physics (2013), *vol.* 79, *part* 5, *pp.* 677–682.
doi:10.1017/S0022377813000299

Interaction of a biased cylinder with a flowing dusty plasma

J. K. MEYER[1], J. R. HEINRICH[2], S.-H. KIM[1] and R. L. MERLINO[1]

[1]Department of Physics and Astronomy, The University of Iowa, Iowa City, IA 52242, USA
(robert-merlino@uiowa.edu)
[2]Air Force Research Laboratory, Kirtland AFB, Albuquerque, NM 87117-5776, USA

(Received 9 January 2013; revised 9 January 2013; accepted 29 January 2013; first published online 6 March 2013)

Abstract. Experimental observations of supersonically flowing dusty plasmas and their interaction with an electrically biased circular cylinder are presented. Two methods for producing flowing dusty plasmas are described. The dusty plasma is produced in a DC anode glow discharge plasma. In Configuration I, a secondary dust cloud, initially formed near a biased grid, flowed away from the grid at supersonic speeds when the grid voltage was suddenly changed. In Configuration II, a pencil-like dust beam was produced using a nozzle-like (converging-diverging) electrostatic potential structure. Using Configuration I, the streaming dust encountered a biased cylinder (wire) whose axis was oriented transverse to the dust flow. The flowing dust particles were repelled by the electrostatic field of the negatively charged cylinder, and a dust void was formed around the cylinder. A detached *electrohydrodynamic* bow shock, akin to the Earth's *magnetohydrodynamic* bow shock, was formed on the upstream side of the cylinder, while an extended teardrop-shaped wake region was formed on the downstream side. Video imaging of the dust stream allowed for observations of the structure and evolution of the bow shock. Configuration II was used to produce a narrow beam of dust particles and observe how the beam was deflected around the biased cylinder. Three multimedia files (movies) of the observed phenomena are provided in the online Supplementary material.

1. Introduction

Fluid flow past a body is one of the fundamental problems in fluid mechanics (Batchelor 1967; Landau and Lifshitz 1987). The flow of a rarefied ionized fluid (plasma) around conducting or non-conducting objects has also been the subject of numerous theoretical and experimental investigations (Stone 1981a, 1981b; D'Angelo and Merlino 1986; Merlino and D'Angelo, 1987) as it relates to the spacecraft–ionosphere interaction problem (Samir 1981; Stone and Samir 1981; Murphy et al. 1989) or to the flow of the solar wind around planets and moons (Luhmann 1986) having no intrinsic magnetic field. The fluid−obstacle interaction problem has also been studied within the context of *electrohydrodynamics* (Melcher and Taylor 1969; Castellanos 1994; Saville 1997; Zhakin 2012), the branch of fluid mechanics dealing with the effects of electric fields on fluids having volume electric charge.

A dusty or complex plasma (Morfill and Ivlev 2009; Shukla and Eliasson 2009) affords an excellent environment in which to study the problem of the interaction of a fluid flow with an obstacle. This is due to the fact that dusty plasmas are often in a liquid-like state and their dynamical behavior can be investigated at the single particle level at high spatial and temporal resolution using laser illumination and video imaging and analysis techniques. Unlike ordinary gases in which atoms or molecules interact via short-range forces, the dust particles are highly charged and interact with each other through electric fields mediated by the plasma. As pointed out by Morfill et al. (2004), these interactions can be more important than other interactions, such as neutral gas drag, so that a dusty plasma can be considered essentially as a one-phase, charged, liquid-like system, thus establishing a connection to the broader field of electrohydrodynamics.

The interaction of moving and stationary objects with flowing or non-flowing dusty plasmas has been studied in the laboratory. Thompson et al. (1999) studied the effect of a stationary or moving metal rod on a dusty plasma. An electrically floating rod inserted into a dusty plasma creates a dust void surrounding the rod since the rod floats to a negative potential and expels negatively charged dust from its immediate region. Thomas et al. (2004) investigated the dependence of the size of the void on the voltage applied to a wire in a dusty plasma. Klindworth et al. (2004) studied dust-free regions around Langmuir probes in an rf-produced dusty plasma under microgravity conditions. Samsonov et al. (1999) observed Mach cones produced in a horizontal layer of dust particles arranged in a hexagonal lattice by a fast dust particle moving in a

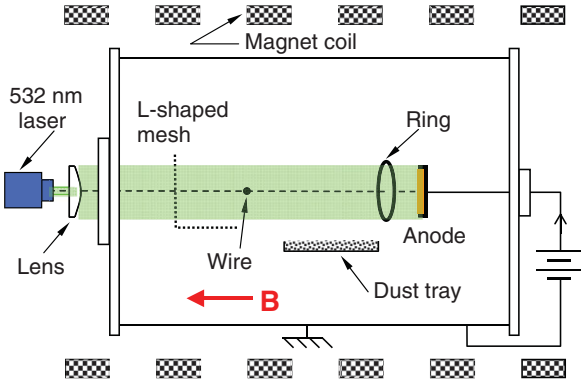

Figure 1. (Colour online) Experimental setup used to produce flowing dusty plasmas. The dusty plasma was formed in a weakly magnetized DC glow discharge between a positively biased circular disk anode and the grounded vacuum vessel walls. In Configuration I, a biased mesh electrode was used to trap a secondary dust cloud, which is then released when the mesh bias voltage was suddenly changed, and then flowed away from the mesh. In Configuration II, a biased ring was placed in front of the anode to form a nozzle-like electrostatic structure that accelerated the dust. Although both the mesh and ring are shown in this figure, each one is used individually.

second incomplete layer beneath the lattice. Morfill et al. (2004) observed the interaction of downward-flowing dust particles with a lentil-shaped void region formed in the center of a dusty plasma that was levitated against gravity by an upward thermophoretic force. The void in this case was produced by dust swept out of a positive region of the discharge by the ion drag force. This was the first study, at the kinetic level, of fluid flow around an obstacle, and showed that the boundary was a 'slip' boundary. Saitou et al. (2012) used a dusty plasma device that could be tilted vertically at various angles to produce a thin two-dimensional layer of dust particles that flowed under the influence of gravity. When the Mach number of the dust flow exceeded 1, they observed the formation of a bow shock in front of a negatively biased wire that protruded perpendicularly through the flowing dust layer.

In this paper, two methods for producing flowing dusty plasmas in a DC glow discharge plasma are described, and qualitative observations of their interaction with electrically biased objects are presented. Three multimedia movies are included in the online Supplementary material to provide a visual record of the dynamic phenomena that are not well represented by still images.

2. Experimental setup and methods

The experiment was performed in a DC glow discharge plasma in argon at 140–150 mTorr. The device, shown schematically in Fig. 1, is a grounded metal cylinder 0.9 m long and 0.6 m in diameter. A set of six water-cooled coils was used to apply an axial magnetic field of a few mT to provide radial confinement for the electrons. A 3.2 cm diameter anode that was movable along the

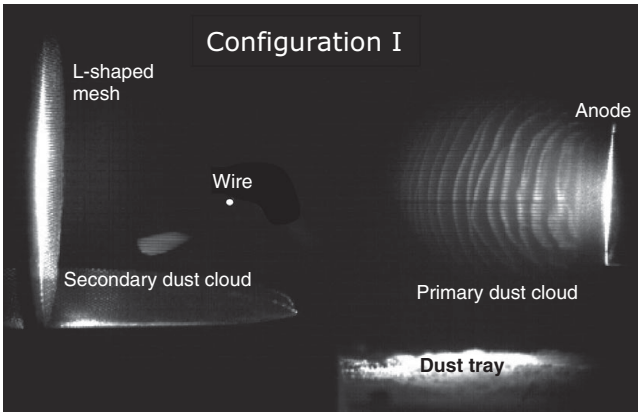

Figure 2. Single frame image of Configuration I, in which a secondary dust cloud was trapped near a biased mesh electrode, and then released when the mesh was suddenly disconnected from ground. The dust cloud then drifted toward the wire.

axis of the device was located near the center of the device. The discharge voltage was in the range of 250 to 300 V, and the discharge current was in the range of 1 to 10 mA. The electric field along the axis of the anode is ~200 V/m, directed away from the anode. A double Langmuir probe was used to measure the electron temperature and ion density, and an emissive probe was used to measure the plasma potential. The electron temperature was in the range of 2 to 4 eV, and the plasma density was in the range of 10^{14} to 10^{15} m^{-3}.

Silica (mass density 1.8 g cm^{-3}) microspheres of one micron diameter, initially resting on an electrically floating tray 2 cm below the anode, entered the plasma naturally when the discharge was turned on. The dust density was typically in the range of ~10^{10} to 10^{11} m^{-3}, and the dust charge, estimated using OML theory, was $Q_d \sim -2000e$. The dust particles were illuminated with a 300 mW, 532 nm, vertical 2 mm thick laser sheet, and the dust dynamics were recorded at up to 500 frames s^{-1} with a Photron (FASTCAM 1024 PCI) CMOS camera, which has a linear response to light intensity, so that the intensity of the light scattered by the dust was proportional to the dust density.

Two independent methods were used to produce flowing dusty plasmas. Configuration I used an L-shaped mesh electrode, while Configuration II used a ring electrode; both configurations are shown schematically in Fig. 1, although only one was used at a time.

2.1. Configuration I

A mesh electrode having an L-shaped cross-section was located about 15 cm from the anode, as shown in Fig. 1. The primary dust cloud was suspended within the anode glow discharge on the right side, and on the left side a secondary dust cloud was trapped in the potential created by the initially grounded mesh electrode. A single frame video image of this configuration is shown in Fig. 2. Dust acoustic waves were present in the primary dust cloud. When the ground connection to the mesh was

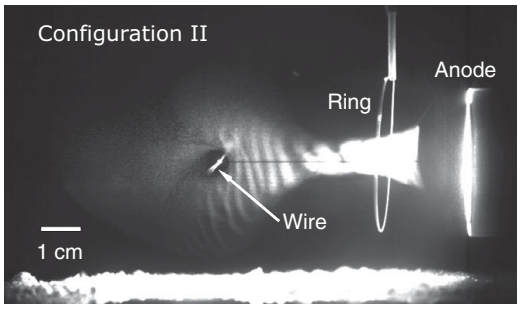

Figure 3. Single frame image of the ring configuration used to control the shape of the dust cloud. By adjusting the position and bias of the ring and the discharge current, the shape and speed of the dust trapped in the anode glow plasma could be changed. In the configuration shown in this figure, a stationary dust cloud was formed, with a void around the negatively biased wire. Under different conditions, the ring and anode configuration produced a nozzle-like structure that accelerated the dust.

removed, and the mesh was allowed to float electrically, the potential well that had confined the secondary dust cloud was removed and the secondary dust cloud was released that began moving toward the anode (Heinrich et al. 2011). Dust acoustic waves, excited by ions drifting away from the anode, were observed both in the primary and secondary dust clouds. In the primary cloud, which was stationary, the dust acoustic waves propagated in the direction of the ion drift, away from the anode. However, in the secondary dust cloud, the dust acoustic waves, as observed in the video images, propagate in the opposite direction, indicating that the flow speed of the secondary cloud was higher than the dust acoustic speed, i.e. the flow was supersonic. From measurements of the speeds of the dust acoustic waves in the secondary and primary clouds, and taking the dust acoustic speed (in the lab frame) as the speed of the waves in the primary cloud, it was estimated that the flow speed of the secondary cloud was about twice the dust acoustic speed, so that the Mach number of the flow was $M \sim 2$. Further experimental details of the trapping and release of the secondary dust cloud and the excitation of dust acoustic waves were reported by Heinrich et al. (2011).

2.2. Configuration II: anode and ring

A 4 cm diameter ring electrode located in front of and coaxial with the anode was used in Configuration II to modify the shape and speed of the dust cloud suspended in the anode glow discharge. By appropriate choices of the controlling parameters (the anode discharge current, ring bias voltage, and ring/anode separation), various electrostatic potential profiles could be formed to change the shape and flow speed of the dust suspension. When the ring was biased to repel dust particles, it acted like a dust aperture, squeezing the dust cloud radially, producing an electrostatic Laval nozzle-like (converging–diverging) potential profile.

Figure 3 shows a single frame video image of the dust cloud using the ring/anode configuration with the ring 2 cm from the anode and biased at −150 V, and with a discharge current of 10 mA. In this case, an approximately 10 cm long, nearly stationary, relatively dense dust cloud was formed, with self-excited dust acoustic waves propagating away from the anode. A 0.5 mm diameter wire that extended across the dust cloud, transverse to the flow, was positioned as a cylindrical obstacle to the dust flow. The wire was biased to repel dust particles, and produced an azimuthally symmetric cylindrical dust void around it, with a sharp gradient in dust density at the void boundary (Wang and Bhattacharjee 2000).

By a different choice of the ring/anode control parameters, Configuration II could also be used to *accelerate* the dust and produce pencil-like dust beams.

3. Observations

In this section, the observations of dust flows and their electrohydrodynamic interaction with a biased wire are presented for Configurations I and II.

3.1. Results using Configuration I

Since the secondary flowing dust cloud in this configuration was transitory, it was possible to observe its entire interaction with the cylinder, from the time of initial incidence until the cloud completely passed over the cylinder. A detached bow shock is expected to form when a supersonic stream is incident on a blunt obstacle (Landau and Lifshitz 1987). Figure 4 shows a sequence of single frame video images of the secondary dust cloud and its interaction with the cylinder (wire) at 48 ms time intervals when the cylinder (wire) was biased at 20 V below the plasma potential. In each image, the secondary dust cloud moves from left to right, and the bright dot in the center of each image is the wire. The image in Fig. 4(a) corresponds to the time when the mesh was switched from grounded to floating, and the secondary cloud was released. Initially, the dust cloud moved impulsively toward the wire at a speed of ∼20 to 25 cms^{-1} (Mach number, M ∼3–4), and a detached bow shock was formed on the front side of the wire, as shown in Fig. 4(c). The flow remained supersonic but slowed down to $\sim 10 - 15$ cm s^{-1}, and the bow shock moved somewhat farther from the wire. The bow shock was identified by measurements of the dust density in front of the wire from Fig. 4(d), as shown in Fig. 5. There is roughly a factor of 3 increase in the dust density on the downstream side of the shock, with a sharp drop in dust density on the upstream side near the wire. A dust density jump of ∼3 is consistent with estimates obtained from the Rankine-Hugoniot relations for M in the range of 1.5 to 2.5. We caution, however, that use of the jump relations requires knowledge of the adiabatic index of the dust fluid, which is not known. The width of the bow shock is ∼1 mm, slightly larger than, but on the order of, the average interparticle spacing, which is estimated to be ∼0.3–0.7 mm. The detached bow shock was formed at approximately 2–3 mm from the wire

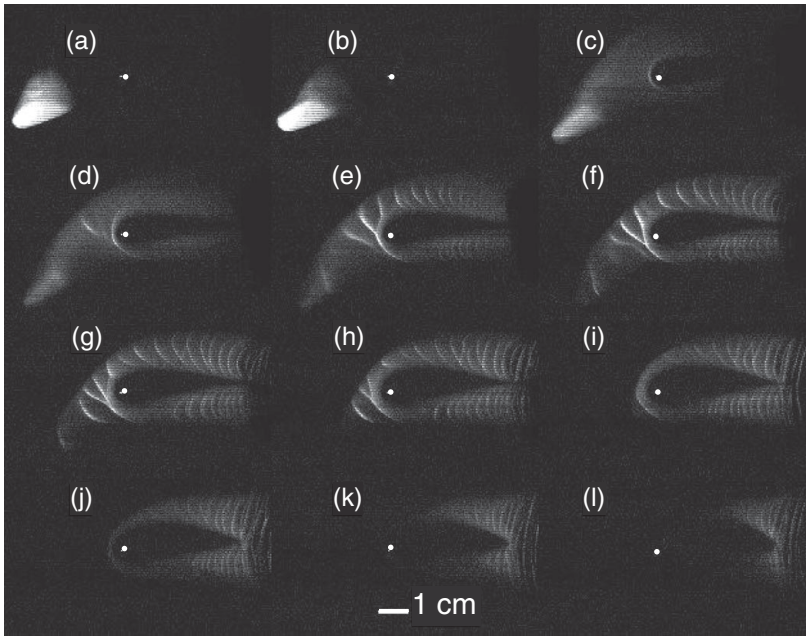

Figure 4. A sequence of single frame images in 48 ms intervals, of the interaction of the flowing secondary dust cloud with the biased wire. The cloud enveloped the wire in the interval between frames (b) and (c), with a bow shock appearing in (c) and fully developed in (d). The flowing dust cloud proceeded downstream of the wire, and an elongated wake was formed that eventually closed by frame (h). The secondary cloud continued to flow downstream, with the rear edge of the cloud passing over the wire by frame (k). A movie of this image sequence is available in the online Supplementary material.

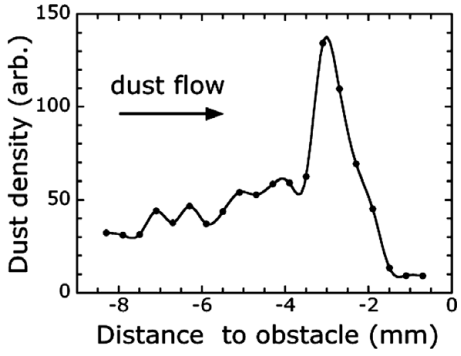

Figure 5. Profile of the dust density jump across the bow shock. The obstacle was at 0 mm.

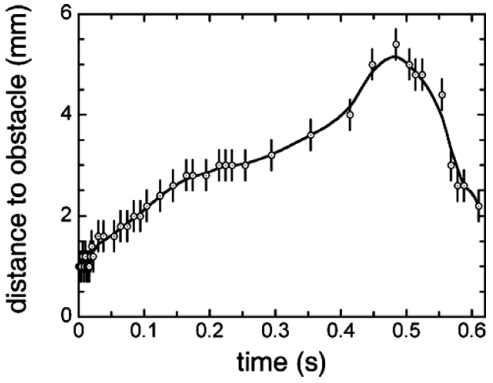

Figure 6. Position of the bow shock with respect to the obstacle vs. time. The shock initially formed very close to the wire, then receded back to an equilibrium position of about 2–3 mm from the wire. For $0.3 < t < 0.45$ s, the flow speed decreased and the bow shock moved farther from the wire. For $t > 0.45$ s, the flow became subsonic and the bow shock disappeared. The data for $t > 0.45$ s give the location of the cloud as it flowed past the wire.

[Fig. 4(f)]. The flow produces a tear drop-shaped wake in the downstream region, which eventually closed by Fig. 4(h). The wake extended out to a distance of about seven times the radius of the obstacle (taken as the void surrounding the wire). Dust acoustic waves appeared in Fig. 4(e), and were carried with the flow, since the flow speed was larger than the dust acoustic speed. Dust acoustic waves propagate, in stationary dust, in the direction of the ion drift, which is away from the anode or toward the mesh. This was evidenced by the curvature of the wavefronts in the secondary cloud (see Heinrich et al. 2011, for further details). As the cloud continued to flow past the wire, the shock began to weaken [Fig. 4(i)] until it was no longer evident [Fig. 4(k)]. The bow shock disappeared when the flow became subsonic, which was identified by the fact that the dust acoustic waves in the trailing portion of the cloud no longer moved in the lab frame. The wake structure remained [4(l)] even after the cloud has moved past the obstacle. [A movie (1) showing the formation and evolution of the bow shock and wake is available in the online Supplementary material.]

The formation and evolution of the bow shock was further investigated from video images obtained at 500 frames s^{-1}. A plot of the position of the bow shock relative to the wire versus time is shown in Fig. 6; the initial time shown corresponds to Fig. 4(c). The streaming dust initially approached to within <0.5 mm from the wire (the ion Debye shielding length was ~0.1 to 0.3 mm), and was then pushed back over the period from 0 to 0.15 s as shown in Fig. 6. From 0.15 to 0.25 s,

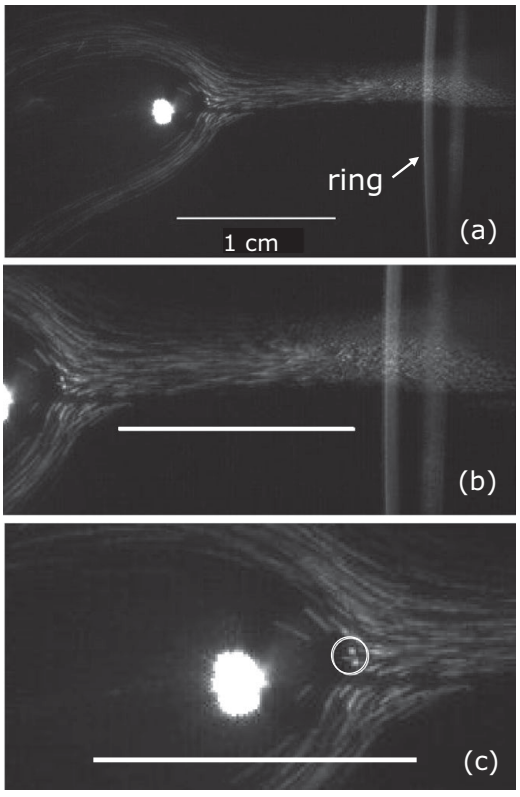

Figure 7. Pencil-like dust stream formed using Configuration II. (a) Single frame large field of view image showing the ring, dust stream, and dust-obstacle interaction. (b) Enlarged view of (a) showing the pencil-like dust beam formed by the ring/anode nozzle configuration. Faster-moving dust in the center of the image appeared as streaklines for the exposure times used. (c) Zoomed-in image of (b) showing details of the stagnation region in front of the wire and particles streaming around the wire. Two nearly stationary particles (within the circle) are seen in the stagnation region just in front of the obstacle.

the bow shock position stabilized at ~2–3 mm from the wire, and then began receding further from the wire (0.25–0.5 s) as the cloud began to slow down. For $t >$ 0.45 s, the trailing edge of the cloud moved passed the wire, and no bow shock was present in this subsonic flow.

3.2. Results using Configuration II

Figure 7(a) shows a single frame image of the dust beam formed using the ring/anode configuration, as it first passed through the ring and then around the cylinder. The conditions used to obtain this image was a discharge current of 2.0 mA, ring voltage of 200 V, and wire voltage of 220 V. [A movie (2) is available in the online Supplementary material.] The anode/ring configuration produced a cylindrical (pencil-like) dust stream with a diameter of about 2 mm and speed of $\sim 10 - 20\,\mathrm{cm\,s^{-1}}$. The frame rate of the video camera used in Fig. 7 was set at 60 frames s^{-1} so that the faster-moving dust grains were not resolved individually, but appeared as streaklines in the images. Figure 7(b) is a close-up view showing the streaklines that began to appear about midway between the ring and the obstacle indicating

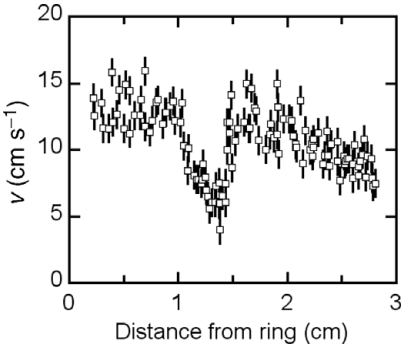

Figure 8. Dust flow speed vs. distance from ring. The obstacle was located at approximately 1.5 cm from the ring.

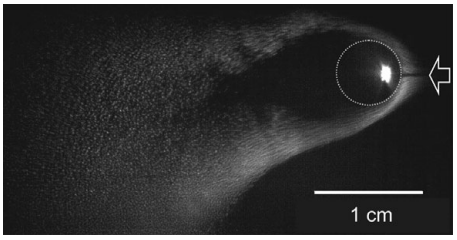

Figure 9. Wake formed behind the obstacle (bright feature on the right side) when a narrow dust beam was incident from the right. The dotted circle indicates the approximate location of the void around the cylinder.

that the dust had been accelerated. The flow speed was determined by reducing the discharge current slightly to 2.0 mA and increasing the camera frame rate to 500 frames s^{-1}, so that individual dust particles could be imaged and tracked over several video frames. Figure 8 shows a plot of the flow speed measured at various distances from the ring. As the particles approached the obstacle, they were slowed down, before being deflected around it.

An even tighter view of the region just in front of the obstacle is shown in Fig. 7(c). In this region, upper and lower particle streams were formed that traveled around the obstacle. A few particles are seen approaching the stagnation point where they were slowed down before passing around the obstacle. Some particles near the beam axis approached closer to the obstacle before passing around it. Occasionally, a few particles were seen approaching directly toward the wire and appeared to vanish. It was possible that these particles penetrated deep into the ion sheath surrounding the wire, and either lost some of their negative charge or may have even acquired a positive charge. This possibility represents a unique feature of the interaction of dust particles, whose charge is not fixed, with a biased object.

Next, we concentrate on the region of interaction of the dust flow with the obstacle and the wake region. Figure 9 shows a single frame video image of the pencil-like dust stream as it encountered the obstacle and was deflected around it forming an elongated wake. [A movie (3) is available in the online Supplementary material.] The conditions for Fig. 9 were: discharge current 2.2 mA,

ring voltage 200 V, and wire voltage 240 V. At a distance of ∼5 mm behind the obstacle, the upper and lower dust streams began to expand and spread into the wake region. The streams flowing around the obstacle were laminar near the cylinder and began to separate from the void (indicated by the dotted circle) at an angle of roughly 90° relative to the direction of the flow. The wake behind the object extended downstream roughly 1.7 cm from the wire, where the upper and lower streams merged as they expanded inward. The Reynolds number, $\mathrm{Re} = U_0\, d/v$ was estimated to be in the range, Re ∼30−300, for flow speeds $U_0 = 10{-}15\,\mathrm{cm\,s^{-1}}$, d ∼3 mm, and a kinematic viscosity $v_d \sim 1 - 10\ \mathrm{mm^2\,s^{-1}}$ (Morfill et al. 2004).

As pointed out by Morfill et al. (2004), the interaction between a flowing dusty plasma and object differs from the prototypical fluid mechanics problem in one important respect. In the latter case the object is a solid that exerts a drag force on the fluid, and the no-slip boundary condition is appropriate. However, in the dusty plasma experiments, the wake boundary is between discreet dust particles and the plasma in the void, so that a 'slip boundary' condition is more likely to be applicable.

4. Conclusions

Two schemes for producing flowing dusty plasmas have been presented in this paper. The first method used a secondary dust cloud that, when released, flowed away from the mesh electrode on which it was initially formed. In the second scheme, the primary dust cloud, which was confined in the potential of the anode glow discharge, was accelerated by a nozzle-like potential configuration formed by a biased ring placed in front of the anode. A narrow, pencil-like dust beam (jet) was formed.

Both configurations were used to study the interaction of streaming dust particles with an obstacle created by the void surrounding a wire biased to repel dust particles. This is similar to the observations reported by Morfill et al. (2004) in which dust flowed around a central lentil-shaped void region of an rf dusty plasma, with one important difference. In the present experiments the void was formed due to the electrostatic repulsion of dust by a negatively biased wire, whereas in the experiments of Morfill et al. (2004) the void was formed by the expulsion of dust by the ion drag force created by ions pushed out of the central positive region of the discharge. The development and evolution of the bow shock formed on the upstream side of the obstacle in the supersonic dust flow were investigated.

The present experiments highlight the feasibility of using dusty or complex plasmas as model systems in which electrohydrodynamic phenomena can be investigated. This is due to the fact that: (a) dusty plasmas can exist in a single-component liquid-like state, and (b) the dynamics of the particles can be studied at the individual particle level using laser illumination and high-speed digital video imaging and analysis techniques.

Acknowledgments

This work was funded by the U.S. Department of Energy Grant No. DE-FG01-04ER54795 and NSF Grant No. PHY-0923141. We thank M. Miller for technical assistance.

Supplementary material

Three movies are available at journals.cambridge.org/flm.

References

Batchelor, G. K. 1967 *An Introduction to Fluid Dynamics*. Cambridge: Cambridge University Press.

Castellanos, A. 1994 Electrohydrodynamics: basic equations and dimensionless numbers. In: *Fluid Physics: Lecture Notes of Summer Schools* (ed. M. G. Velarde and C. I. Christov). Madrid: World Scientific, pp. 14–32.

D'Angelo, N. and Merlino, R. L. 1986 *IEEE Trans. Plasma Sci.* **PS-14**, 609.

Heinrich, J. H., Kim, S.-H., Meyer, J. and Merlino, R. L. 2011 *Phys. Plasmas* **18**, 113706.

Klindworth, M., Piel, A., Melzer, A., Konopka, U., Rothermel, H., Taranik, K. and Morfill, G. E. 2004 *Phys. Rev. Lett.* **93**, 195002.

Landau, L. D. and Lifshitz, E. M. 1987 *Fluid Mechanics*, 2nd edn. Oxford: Pergamon Press.

Luhmann, J. G. 1986 *Space Sci. Rev.* **44**, 41.

Melcher, J. R. and Talyor, G. I. 1969 *Ann. Rev. Fluid Mech.* **1**, 111.

Merlino, R. L. and D'Angelo, N. 1987 *J. Plasma Phys.* **37**, 185.

Morfill, G. E. and Ivlev, A. V. 2009 *Rev. Mod. Phys.* **81**, 1354.

Morfill, G. E., Rubin-Zuzic, M., Rothermel, H., Ivlev, A. V., Klumov, B. A., Thomas, H. M. and Konopka, U. 2004 *Phys. Rev. Lett.* **92**, 175004.

Murphy, G. B., Reasoner, D. L., Tribble, A., D'Angelo, N., Pickett, J. S. and Kurth, W. S. 1989 *J. Geophys. Res.* **94**, 6866.

Saitou, Y., Nakamura, Y., Kamimura, T. and Ishihara, O. 2012 *Phys. Rev. Lett.* **108**, 065004.

Samir, U. 1981 *Adv. Space Res.* **1**, 373.

Samsonov, D., Goree, J., Ma, Z. W., Bhattacharjee, A., Thomas, H. M. and Morfill, G. E. 1999 *Phys. Rev. Lett.* **83**, 3649.

Saville, D. A. 1997 *Ann. Rev. Fluid Mech.* **29**, 27.

Shukla, P. K. and Eliasson, B. 2009 *Rev. Mod. Phys.* **81**, 25.

Stone, N. H. 1981a *J. Plasma Phys.* **25**, 351.

Stone, N. H. 1981b *J. Plasma Phys.* **26**, 385.

Stone, N. H. and Samir, U. 1981 *Adv. Space Res.* **1**, 361.

Thomas, E., Jr., Avinash, K. and Merlino, R. L. 2004 *Phys. Plasmas* **11**, 1770.

Thompson, C. O., D'Angelo, N. and Merlino, R. L. 1999 *Phys. Plasmas* **6**, 1421.

Wang, X. and Bhattacharjee, A. 2000 *Phys. Plasmas* **7**, 3093.

Zhakin, A. I. 2012 *Phys.–Uspekhi* **55**, 465.